Impact of Inverter-Based Generation on Islanding Detection Schemes in Distribution Networks

Uros Markovic*, Demetris Chrysostomou*, Petros Aristidou†, Gabriela Hug*
* EEH - Power Systems Laboratory, ETH Zurich, Physikstrasse 3, 8092 Zurich, Switzerland
† Department of Electrical Engineering, Computer Engineering and Informatics,
Cyprus University of Technology, Archiepiskopou Kyprianou 30, 3036 Limassol, Cyprus

***Abstract*—One of the most frequently used interface protections for Distributed Generators (DGs) is the Loss of Mains (LoM) protection. It detects the formation of an island at the connection point and disconnects the DG to protect the unit, the system and the personnel. The increased penetration of inverter-interfaced DG, in combination with the decommissioning of synchronous generators, reduces the system inertia and leads to faster changing and larger voltage and frequency deviations. Therefore, modern grid-codes require inverter-based DGs to provide support to the grid by modifying their active and reactive power injection based on local measurements. However, this leads to complex inverter-grid interactions and modifies the islanded system behavior, thus disturbing the operation of LoM protections that rely mainly on local voltage and frequency measurements. In this paper, we propose an improved analytical formulation for estimating the Non-Detection Zone (NDZ) of LoM protection devices in the presence of grid-feeding inverters, as well as novel NDZ approximations for grid-supporting and grid-forming inverter-based services. We verify the analytical results with detailed dynamic simulations and comment on the impact that the new inverter requirements have on the performance of LoM protections.**

***Index Terms*—Non-detection zone, loss of mains, analytical approximation, grid-forming, grid-following**

I. Introduction

The growing penetration of Distributed Generation (DG) in power systems poses new challenges related to protection and control of these units. One of the most important aspects and a primary concern for operators in such systems is the occurrence of unintentional islanding or so-called Loss of Mains (LoM), where a DG unit is disconnected from the main utility grid but continues to operate and energize an isolated portion of the system. Such operating conditions are highly undesirable as they complicate the orderly reconnection of the utility network and pose a hazard to the utility system and personnel, other customers, and to the DG itself. In addition to its normal function of protection and control of the DG, a state-of-the-art converter control scheme should be able to provide reliable islanding detection and cease to energize the area, typically within two seconds of the islanding instance, as prescribed by the IEEE 1547 standard [1].

With the share of distributed renewable generation steadily increasing, the degree of DG capacity is becoming sufficiently large to supply the local load demand and therefore reduce the power drawn from the grid. Under such circumstances the risk of LoM detection failure becomes particularly high, with the protection inputs - usually related to frequency and voltage deviations - not being large enough for detecting islanding within a prescribed time period. The Non-Detection Zone (NDZ) is frequently used as a protection performance index defined in terms of active/reactive ($\Delta P/\Delta Q$) power mismatch between the DG inverter and the load. In particular, NDZ determines the minimum values of power mismatch between local load and generation that would trigger the LoM protection schemes. The islanding detection algorithm with the smallest NDZ is thus considered as the most effective.

The existing anti-islanding techniques can be categorized into local and remote, with local schemes being further classified into active and passive [2]–[5]. Active schemes are generally based on the concept of perturb and observe [4], [6], where an external signal is injected into the system for the purpose of perturbing the DG output parameters up to a significant level upon islanding occurrence. While this deviation is relatively insignificant in normal operation, it would drastically enlarge in case of LoM and trip the protection relays. Passive methods use only local voltage and current sensing to detect abnormal operation while monitoring system characteristics such as Over/Under- Voltage (OV/UV) and Frequency (OF/UF), Rate-of-Change-of-Frequency (RoCoF), and voltage phase jumps [5]. Therefore, they possess a larger NDZ compared to active methods. However, while generally more effective, the active schemes are also slower, more expensive, tend to deteriorate power quality, reduce efficiency of parallel inverters, and may potentially have adverse impact on grid dynamics and lead to instability [7]. Finally, remote LoM methods connect the DGs directly to the feeder relays through inter-tripping mechanisms and are the most accurate and robust. However, they require protection-grade communication infrastructure and advanced signal processing techniques for every DG, which is usually not available and expensive to install. Despite having negligible NDZ and high reliability in comparison with local schemes, high cost, complexity, and implementation problems lead to local schemes being more preferable [3]. Therefore, in this work, we solely focus on local passive protection schemes, in particular the detection algorithms based on over/under-voltage and over/under-frequency measurements [8].

The existing literature focuses solely on anti-islanding protection of *grid-feeding* inverters [8]–[13], and the suggested approximations of NDZs tend to be imprecise due to unjustified physical assumptions. In particular, the proposed analytical expressions yield a rectangular NDZ (e.g., see [8]–[10]), whereas the simulations and real-world measurements indicate a rather trapezoidal-shaped non-detection region [8]. Such imprecision is a consequence of often neglected dependencies between the active power and frequency, i.e., reactive power and voltage, respectively, which simplifies the mathematical analysis of the problem at hand. Moreover, considering that the more compelling converter control modes such as *grid-forming* and *grid-supporting* are gradually emerging [14], the compatibility of traditional LoM detection schemes needs to be re-evaluated.

This paper tackles the weaknesses of the existing analytical NDZ approximations applied to passive UV/OV and UF/OF anti-islanding protection schemes of grid-feeding inverters in [8]–[13], and proposes a more accurate formulation which achieves an almost perfect match with the simulations. More-

over, we extend the framework onto more complex inverter control schemes, namely grid-feeding and grid-supporting, and derive the analytical approximations for their respective NDZs. To the best knowledge of the authors, such formulation has not yet been presented in the literature. Finally, the theoretical results have been verified through simulations using a detailed inverter control model connected to a distribution grid, as prescribed by industry standards.

The remainder of the paper is structured as follows. In Section II, the standard anti-islanding testing conditions are presented, together with the existing practice for deriving the analytical NDZ approximation of grid-feeding inverters. Furthermore, the improved mathematical formulation for grid-feeding NDZ is introduced, followed by the derivation of novel NDZ expressions for grid-feeding and grid-supporting operation modes. Section III discusses the modeling and implementation of different converter control schemes as well as the design and settings of LoM protection schemes. The proposed theoretical approach is validated through time-domain simulations in Section IV, whereas Section V discusses the outlook of the study and concludes the paper.

II. Analytical Approximation of NDZ

A. Anti-Islanding Testing Conditions

A generic system traditionally used for LoM studies is illustrated in Fig. 1, as defined by the IEEE 1547 standard. Testing conditions of the RLC load are as follows: (i) resonant load frequency is the same as grid frequency; (ii) load quality factor[1] is set to $Q_f = 2.5$; and (iii) power generated by DG should match the power consumed by the load, i.e., $\Delta P = \Delta Q = 0$ when switch S_2 is closed. Under such conditions, the opening of switch S_2 results in resonance at nominal voltage and frequency between the islanded DG and load. The DG operating with unity power factor (i.e., $Q_G = 0$) yields a worst-case scenario for islanding detection (see [8]) and will therefore be considered as benchmark in this study.

In reality, there is always some power mismatch $(\Delta P, \Delta Q)$ between the DG output and the load, compensated by the network when operating in grid-connected mode. Therefore, after the grid disconnection, the voltage and frequency in the system are forced to new values $\hat{V}$ and $\hat{f}$, respectively. In case of a large power mismatch, these values might exceed the permissible ranges of the voltage and frequency protection schemes, which would in turn trip the switch S_1 to prevent continued islanded operation. The general relationship between the power mismatch and the voltage/frequency thresholds can be expressed as follows:

$$g\left(V, V_{\max}, \Delta Q\right) \leq \frac{\Delta P}{P_G} \leq g\left(V, V_{\min}, \Delta Q\right), \tag{1a}$$

$$h\left(f, f_{\min}, Q_f, \Delta P\right) \leq \frac{\Delta Q}{P_G} \leq h\left(f, f_{\max}, Q_f, \Delta P\right), \tag{1b}$$

where $V_{\min}$, $V_{\max}$, $f_{\min}$ and $f_{\max}$ are the respective UV/OV and UF/OF thresholds, typically defined as percentages of nominal voltage and frequency, and P_G is the DG's active power before the islanding event used as a normalization constant. The area formed in the $\Delta P - \Delta Q$ plane by the expressions in (1) is defined as NDZ, and it indicates a set of power mismatches for which an island may be formed without being detected. More precisely, for any power mismatch within the specified thresholds the resulting voltage and frequency in the system will remain within the nominal range, even after a grid disconnection, thus failing to trigger the LoM protection.

[1]The quality factor is defined as the ratio of the reactive power stored in the L and C elements and the active power consumed by the resistance R.

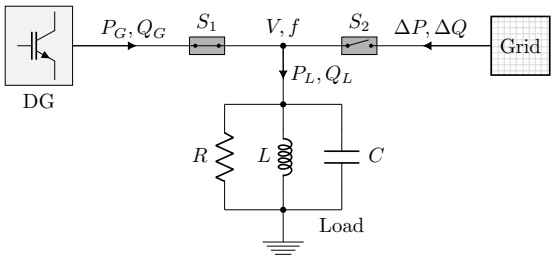

Fig. 1. Generic system for studying anti-islanding detection schemes.

B. Existing Practice

The existing literature is confined within the scope of DGs controlled as a constant power source, i.e., interfaced to the grid via an inverter operating in a so-called grid-feeding mode [8]–[13]. This implies that the injected power from a DG remains the same before and after an islanding event, which drastically simplifies the analysis. Moreover, the $\Delta P - f$ and $\Delta Q - V$ dependencies are often neglected, resulting in a rectangular NDZ approximation with vertical and horizontal lines coming from the voltage and frequency thresholds in (1a) and (1b), respectively. Such analytical formulation can be derived by looking at the power balance before and after the grid disconnection, as previously described in [8]–[10] and derived hereinafter.

Let us denote by $\hat{}$ the quantities after the LoM event. Having in mind that $\hat{P}_G = \hat{P}_L$ and $\hat{Q}_G = \hat{Q}_L$, one obtains:

$$\Delta P \coloneqq P_L - P_G = \Delta P_G - \Delta P_L, \tag{2a}$$

$$\Delta Q \coloneqq Q_L - Q_G = \Delta Q_G - \Delta Q_L, \tag{2b}$$

where $\Delta P_i \coloneqq \hat{P}_i - P_i$ and $\Delta Q_i \coloneqq \hat{Q}_i - Q_i$, $\forall i \in \{G, L\}$. For the grid-feeding case at hand, the DG power after the event remains (or almost instantaneously restores to) the same power, i.e., $\Delta P_G = \Delta Q_G = 0$. On the other hand, the load consumption varies due to a change in voltage and frequency:

$$P_L = \frac{V^2}{R}, \quad Q_L = V^2\left(\frac{1}{\omega L} - \omega C\right), \tag{3a}$$

$$\hat{P}_L = \frac{\hat{V}^2}{R}, \quad \hat{Q}_L = \hat{V}^2\left(\frac{1}{\hat{\omega} L} - \hat{\omega} C\right), \tag{3b}$$

with $\omega = 2\pi f$ and $\hat{\omega} = 2\pi \hat{f}$. Since $\Delta P_G = 0$ and $P_G = \hat{P}_G = \hat{P}_L$, one can describe the $\Delta P / P_G$ term using the expressions in (3) by

$$\frac{\Delta P}{P_G} = -\frac{\Delta P_L}{P_G} = -\frac{\Delta P_L}{\hat{P}_L} = \frac{\left(V^2 - \hat{V}^2\right)/R}{\hat{V}^2/R} = \frac{V^2}{\hat{V}^2} - 1. \tag{4}$$

Therefore, for the voltage $\hat{V}$ to be kept within $[V_{\min}, V_{\max}]$ limits, the following condition must be satisfied:

$$\frac{V^2}{V_{\max}^2} - 1 \leq \frac{\Delta P}{P_G} \leq \frac{V^2}{V_{\min}^2} - 1, \tag{5}$$

which yields two vertical lines in the $\Delta P - \Delta Q$ NDZ plane, as previously discussed.

A slightly different approach is taken for deriving the reactive power mismatch bounds. Since the DG power factor is assumed to be 1, we can set $Q_G = 0$ and therefore $\Delta Q = Q_L$. Moreover, according to the IEC 62116:2014 standard [15] and

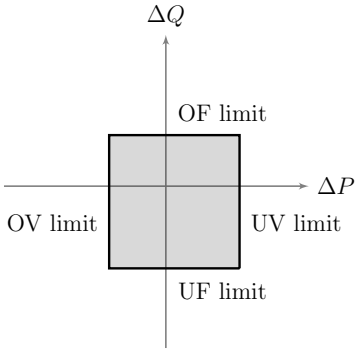

Fig. 2. Graphical illustration of the (traditional) NDZ approximation widely used in the literature.

without loss of generality, the load is initialized at resonant frequency $f = 1/\left(2\pi\sqrt{L_0 C_0}\right)$, where L_0 and C_0 are the respective resonant frequency components and the quality factor is equal to $Q_f = RL_0/C_0$. Subsequently, either L or C load component is changed to accommodate for $\Delta Q \neq 0$, which holds as long as $Q_f \geq \Delta Q/P_G$. For the purposes of this study, we will assume that the capacitive element yields the complete reactive power mismatch, i.e.,

$$L = L_0\,, \quad C = C_0 + \Delta C = C_0 - \frac{\Delta Q}{2\pi f V^2}\,, \tag{6}$$

which together with (3) and the fact that $\Delta Q = Q_L$ results in

$$\Delta Q = Q_L = V^2\left(\frac{1}{2\pi f L_0} - 2\pi f\left(C_0 + \Delta C\right)\right). \tag{7}$$

By combining the expressions (2b)-(3b), (6) and (7), and conducting a set of trivial mathematical operations, one obtains:

$$\frac{\Delta Q}{P_G} = Q_f\left(1 - \frac{f^2}{\hat{f}^2}\right), \tag{8}$$

which gives the NDZ bounds on the reactive power mismatch of the form:

$$Q_f\left(1 - \frac{f^2}{f_{\min}^2}\right) \leq \frac{\Delta Q}{P_G} \leq Q_f\left(1 - \frac{f^2}{f_{\max}^2}\right). \tag{9}$$

The thresholds in (9) define two horizontal lines in the $\Delta P - \Delta Q$ plane and together with (5) complete the rectangular-shaped NDZ illustrated in Fig. 2, characteristic of grid-feeding DG units. However, while widely used in the literature, such approximation tends to be inaccurate when compared to simulations and experimental studies, as previously pointed out in [8]. The imprecision mostly arises from simplifications based on ignoring the $\Delta P - f$ and $\Delta Q - V$ dependencies. Furthermore, the existing NDZ formulation is applicable only to a single mode of operation. With grid-feeding control design being replaced by more complex grid-forming and grid-supporting control schemes [14], a need for a comprehensive analytical NDZ evaluation that encompasses all potential DG control modes is rapidly increasing. In the remainder of this section, we will introduce the aforementioned inverter operation modes, followed by a novel formulation of NDZ thresholds for each inverter mode respectively.

C. Converter Operation Modes

Depending on their operation in a system, power converters can be classified into grid-forming and grid-following, with the latter category further distinguishing between grid-feeding and grid-supporting units [14]. The conceptual differences come mostly from the power control design (i.e., the outer control loop) and the input/output characteristic of the respective controller, as illustrated in Fig. 3. In particular, grid-forming converters can be represented as an ideal AC voltage source with a low-output impedance, setting the voltage amplitude V and frequency f at the connection terminal by adjusting the predefined power setpoints $(P_G^\star, Q_G^\star)$ using a droop control law of the form:

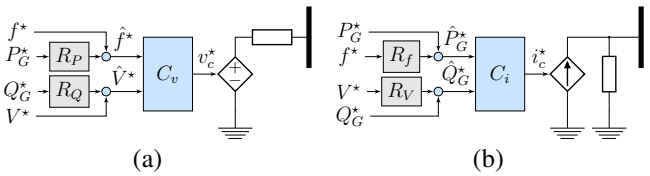

Fig. 3. Simplified representation of grid-connected power converters with characteristic setpoint input and internally computed reference output: (a) grid-forming mode; and (b) grid-following mode.

$$\hat{f}^\star \coloneqq f^\star + R_P\left(P_G^\star - \hat{P}_G\right) = f^\star - R_P\Delta P, \tag{10a}$$

$$\hat{V}^\star \coloneqq V^\star + R_Q\left(Q_G^\star - \hat{Q}_G\right) = V^\star - R_Q\Delta Q, \tag{10b}$$

with $\hat{f}^\star$ and $\hat{V}^\star$ denoting the internally computed frequency and voltage references, and R_P and R_Q being the active and reactive power droop gains respectively. Therefore, these converters are capable of operating in an islanded network without the presence of traditional synchronous generators.

On the other hand, the grid-following power converters are mainly designed to deliver power to an energized grid. They can be represented as an ideal current source connected to the grid in parallel with a high impedance. While the grid-feeding mode acts as a constant power source with a fixed power output $P_G = P_G^\star$ and $Q_G = Q_G^\star$, the grid-supporting operation in addition regulates the current and voltage at the converter output in order to keep the grid frequency and voltage amplitude close to the nominal values, as follows:

$$\hat{P}_G^\star \coloneqq P_G^\star + R_f\left(f^\star - \hat{f}\right) = P_G^\star - R_f\Delta f, \tag{11a}$$

$$\hat{Q}_G^\star \coloneqq Q_G^\star + R_V\left(V^\star - \hat{V}\right) = Q_G^\star - R_V\Delta V, \tag{11b}$$

where $\hat{P}_G^\star$ and $\hat{Q}_G^\star$ are the adjusted power output references, and R_f and R_V denote the frequency and voltage-related droop gains. The operation of grid-following converters is contingent on having a stiff frequency signal at the connection terminal, which is then measured via a Phase-Locked Loop (PLL) and used for power regulation. Hence, these converter units do not posses standalone capabilities.

The system-level controllers C_v and C_i combine the signals and provide respective reference vectors $v_c^\star \in \mathbb{R}^2$ and $i_c^\star \in \mathbb{R}^2$ to device-level control, that adjusts the converter output accordingly. Therefore, in steady state, the equalities $\hat{f} = \hat{f}^\star$ and $\hat{V} = \hat{V}^\star$ hold for the grid-forming converter, i.e., $\hat{P}_G = \hat{P}_G^\star$ and $\hat{Q}_G = \hat{Q}_G^\star$ for the grid-following converter. Note that all state-of-the-art system-level control schemes (e.g., virtual synchronous machine and virtual oscillator control) are subsumed under the droop control in steady state [16]. Understandably, the device-level control (i.e., inner control loop) design also varies between different operation modes, which will be discussed in Section III-A. In particular, the grid-forming mode comprises a cascade of voltage and current PI controllers, whereas the grid-following mode only employs the

current control. More details on both the system- and device-level control are provided in [14], [16]–[19].

D. NDZ Approximation for Grid-Following DGs

In this section, we focus on deriving the analytical expressions for NDZ approximation of a DG controlled through a grid-following inverter. In particular, we will focus on the grid-supporting mode, since a corresponding approximation for the grid-feeding case can be easily obtained by setting the droop gains R_f and R_V to zero. Based on the previously introduced notation and according to (11), we can determine the change in DG's active and reactive power as

$$\Delta P_G = -R_f \Delta f, \quad \Delta Q_G = -R_V \Delta V. \tag{12}$$

Combining it with (3) and using the same procedure as in Section II-B, the expression for normalized active power change $\Delta P/P_G$ is obtained:

$$\frac{\Delta P}{P_G} = \frac{V^2}{\hat{V}^2} - 1 - \frac{V^2 R_f \big(\hat{f} - f\big)}{\hat{V}^2 P_G}. \tag{13}$$

The approach for deriving the reactive power mismatch bounds is again similar to the one presented in Section II-B, i.e., we assume a unity DG power factor and therefore set $Q_G = 0$ and $\Delta Q = Q_L$. Accordingly, using (3b) and (11a) we derive

$$R_V \Delta V = -\hat{V}^2 \left(\frac{1}{2\pi \hat{f} L_0} - 2\pi \hat{f} \left(C_0 + \Delta C \right) \right), \tag{14}$$

which substituted into (6) yields

$$\frac{\Delta Q}{P_G} = \left(1 + \frac{\Delta P}{P_G}\right) \left(Q_f \left(1 - \frac{f^2}{\hat{f}^2} \right) - R R_V \frac{f \Delta V}{\hat{f} \hat{V}^2} \right). \tag{15}$$

The formulation in (13) and (15) clearly corresponds to (4) and (8) from Section II-B. However, unlike (4) and (8), the expressions in (13) and (15) are dependent on $\hat{V}$ and $\hat{f}$ respectively, which is not in accordance with the definition of $g(\cdot)$ and $h(\cdot)$ in (1). Therefore, relationships describing $\hat{f}(V, \hat{V})$ and $\hat{V}(f, \hat{f})$ have to be derived and substituted into (13) and (15).

Let us rewrite (13) and (14) using (2)-(3), as follows:

$$R_f \Delta f = -\frac{\hat{V}^2}{R} + P_G, \tag{16a}$$

$$R_V \Delta V = -\hat{V}^2 \left(\frac{1}{2\pi \hat{f} L} - 2\pi \hat{f} C \right). \tag{16b}$$

By solving (16a) for $\hat{f}$ and (16b) for $\hat{V}$, and embedding the power output limits, we obtain

$$\hat{f}\left(V, \hat{V}\right) = \frac{1}{4\pi C} \left(\frac{R_V \Delta V}{\hat{V}^2} + \sqrt{\left(\frac{R_V \Delta V}{\hat{V}^2} \right)^2 + 4 \frac{C}{L}} \right), \tag{17a}$$

$$\hat{V}\left(f, \hat{f}\right) = \sqrt{R \left(\min\Big\{ P_{\text{nom}}, \max\big\{0, P_G - R_f \Delta f\big\} \Big\} \right)}, \tag{17b}$$

where P_{nom} denotes the nominal (rated) power of the inverter and "min" and "max" terms ensure that the DG power output is within the permissible range $\hat{P}_G \in [0, P_{\text{nom}}]$. Interestingly enough, the relationship in (17a) somewhat resembles the definition of "islanding pulsation" from [4] and [9].

The next step towards a general formulation (1) is to eliminate the load parameters from (17). Each RLC combination reflects a different power mismatch between the load and DG prior to the LoM event. Hence, NDZ is simulated through small perturbations of load parameters and evaluating whether the protection is able to detect the islanding for each scenario. For simplicity and without loss of generality, we assume that the inductive load element provides the complete inductive power mismatch. Substituting $\Delta C = 0$ into (7) and solving for L yields

$$L = \frac{1}{2\pi f} \left(\frac{\Delta Q}{V^2} + 2\pi f C_0 \right)^{-1}, \tag{18}$$

which in turn transforms (17a) into

$$\hat{f}(V, \hat{V}, \Delta Q) = \frac{\beta_V + \sqrt{\beta_V^2 + 8\pi f C_0 \left(\frac{\Delta Q}{\hat{V}^2} + 2\pi f C_0 \right)}}{4\pi C_0}, \tag{19}$$

with the introduction of new variable $\beta_V = R_V \frac{\Delta V}{\hat{V}^2}$. Note that the load is initialized at resonant frequency $f = \frac{1}{2\pi\sqrt{L_0 C_0}}$.

As for the resistive component, by combining (2a) and (3a) we can describe the load resistance as $R = \frac{V^2}{\Delta P + P_G}$, which substituted into (17b) gives

$$\hat{V}(f, \hat{f}, \Delta P) = \sqrt{\frac{V^2}{\Delta P + P_G} \left(\min\Big\{ P_{\text{nom}}, \hat{P}_G \Big\} \right)}. \tag{20}$$

Here, $\hat{P}_G = \max\big\{0, P_G - R_f \Delta f\big\}$ denotes the active power output of the DG after the disconnection, bounding $\hat{P}_G \in [0, P_{\text{nom}}]$ similarly to (17b).

The NDZ approximation can therefore be represented by the following inequalities:

$$\min_{\hat{V}} g\big(V, \hat{V}, \Delta Q\big) \leq \frac{\Delta P}{P_G} \leq \max_{\hat{V}} g\big(V, \hat{V}, \Delta Q\big), \tag{21a}$$

$$\min_{\hat{f}} h\big(f, \hat{f}, \Delta P\big) \leq \frac{\Delta Q}{P_G} \leq \max_{\hat{f}} h\big(f, \hat{f}, \Delta P\big), \tag{21b}$$

where $g(\cdot)$ and $h(\cdot)$ are obtained by substituting (19) into (13) and (20) into (15), respectively. Such mathematical procedure finalizes the NDZ approximation and yields

$$\frac{V^2}{V_{\max}^2} - 1 - \frac{V^2 R_f \Delta f_1}{V_{\max}^2 P_G} \leq \frac{\Delta P}{P_G} \leq \frac{V^2}{V_{\min}^2} - 1 - \frac{V^2 R_f \Delta f_2}{V_{\min}^2 P_G}, \tag{22a}$$

$$\xi_{\min} \leq \frac{\Delta Q}{P_G} \leq \xi_{\max}, \tag{22b}$$

with the NDZ bounds for reactive power described by

$$\xi_{\min} \coloneqq \left(1 + \frac{\Delta P}{P_G}\right) \left(Q_f \left(1 - \frac{f^2}{f_{\min}^2} \right) - R R_V \frac{f \Delta V_1}{f_{\min} \hat{V}_1^2} \right),$$

$$\xi_{\max} \coloneqq \left(1 + \frac{\Delta P}{P_G}\right) \left(Q_f \left(1 - \frac{f^2}{f_{\max}^2} \right) - R R_V \frac{f \Delta V_2}{f_{\max} \hat{V}_2^2} \right).$$

The deviation terms in (22) are defined $\forall i \in \{1, 2\}$ as

$$\Delta f_i \coloneqq \hat{f}_i - f, \quad \Delta V_i \coloneqq \hat{V}_i - V, \tag{23}$$

whereas the newly introduced variables are of the form

$$\hat{f}_1 \coloneqq \hat{f}\big(V, V_{\max}, \Delta Q\big), \quad \hat{f}_2 \coloneqq \hat{f}\big(V, V_{\min}, \Delta Q\big), \tag{24a}$$

$$\hat{V}_1 \coloneqq \hat{V}\big(f, f_{\min}, \Delta P\big), \quad \hat{V}_2 \coloneqq \hat{V}\big(f, f_{\max}, \Delta P\big). \tag{24b}$$

The mathematical justification for selecting $g_{\min}(\cdot, V_{\max})$, $g_{\max}(\cdot, V_{\min})$ and $h_{\min}(\cdot, f_{\min})$, $h_{\max}(\cdot, f_{\max})$ is based on the monotonic properties of the nonlinear functions $g(\cdot)$ and $h(\cdot)$ and is given in the Appendix. Unlike the traditional practice presented in Section II-B, where only $\Delta P - V$ and $\Delta Q - f$ dependencies are considered when approximating the NDZ, the proposed formulation also captures the impact of one power mismatch on another, i.e., incorporates the correlation between the $(\Delta P, f)$ and $(\Delta Q, V)$ terms.

Revisiting the conceptual differences between the grid-feeding and grid-supporting mode of operation elaborated in Section II-C, one can easily approximate the NDZ of a grid-feeding converter by setting $R_f = R_V = 0$ in (22), which results in

$$\frac{V^2}{V_{\max}^2} - 1 \leq \frac{\Delta P}{P_G} \leq \frac{V^2}{V_{\min}^2} - 1, \tag{25a}$$

$$(K_P + 1)Q_f \beta_{f_{\min}} \leq \frac{\Delta Q}{P_G} \leq (K_P + 1)Q_f \beta_{f_{\max}}, \tag{25b}$$

with $K_P = \Delta P / P_G$ and the new function $\beta_{\hat{f}} = 1 - f^2/\hat{f}^2$.

Comparing the analytical bounds in (25) to (5) and (9) respectively, we can conclude that the proposed formulation improves the approximation of the under/over-frequency thresholds of a greed-feeding inverter. In particular, it introduces a $(1 + \Delta P/P_G)$ term and therefore a linear dependency between the frequency and active power mismatch described in (25b), which breaks the traditional hierarchy of rectangular-shaped NDZs that do not accurately capture the realistic system conditions. More precisely, (25b) introduces a gradient in the bounds describing the UF/OF triggers in the $\Delta P - \Delta Q$ plane, which in turn yields a trapezoidal NDZ, as will be shown in Section IV.

E. NDZ Approximation for Grid-Forming DGs

While conceptually different in operation principles, the mathematical representation of the outer control loops of the grid-forming and grid-supporting converters has many similarities due to a droop-based control law. As a matter of fact, by comparing (10a) and (11a), i.e., (10b) and (11b), we can conclude that the two sets of expressions are identical if $R_P = R_f^{-1}$ and $R_Q = R_V^{-1}$. Therefore, the analytical approximation of NDZ for the grid-forming mode of operation can be obtained through minor alteration of the previously derived formulation for the grid-supporting converter. Indeed, the bounds of the non-detection region can also be expressed by (22), where R_f and R_V are replaced by R_P^{-1} and R_Q^{-1} respectively. Hence, the analytical approximation of the NDZ for a grid-forming inverter is of the form:

$$\frac{V^2}{V_{\max}^2} - 1 - \frac{V^2 \Delta f_1}{V_{\max}^2 R_P P_G} \leq \frac{\Delta P}{P_G} \leq \frac{V^2}{V_{\min}^2} - 1 - \frac{V^2 \Delta f_2}{V_{\min}^2 R_P P_G}, \tag{26a}$$

$$\gamma_{\min} \leq \frac{\Delta Q}{P_G} \leq \gamma_{\max}, \tag{26b}$$

where the NDZ bounds for reactive power are defined by

$$\gamma_{\min} \coloneqq \left(1 + \frac{\Delta P}{P_G}\right)\left(Q_f\left(1 - \frac{f^2}{f_{\min}^2}\right) - \frac{Rf\Delta V_1}{R_Q f_{\min} \hat{V}_1^2}\right),$$

$$\gamma_{\max} \coloneqq \left(1 + \frac{\Delta P}{P_G}\right)\left(Q_f\left(1 - \frac{f^2}{f_{\max}^2}\right) - \frac{Rf\Delta V_2}{R_Q f_{\max} \hat{V}_2^2}\right).$$

The exploration of monotonic properties of $g(\cdot)$ and $h(\cdot)$ for the grid-supporting mode, discussed in the Appendix, applies to the grid-forming control mode as well.

III. Modeling & Implementation

A. Converter Control Design

We consider a state-of-the-art VSC control scheme previously described in [16]–[20], where the outer control loop consists of droop-based active and reactive power controllers providing either voltage angle and magnitude (grid-forming) or active and reactive power references (grid-following) by adjusting the predefined setpoints (denoted by $x^\star$) according to a measured power, voltage and/or frequency imbalance. Subsequently, the computed reference signals (denoted by x_{ref}) are passed through the inner control loop to adjust the inverter output. In the grid-forming case, the inner loop is comprised of cascaded voltage and current controllers, whereas for the grid-following operation mode the power references are directly fed to the current controller. It should be noted that the latter inverter type has two implementations: a constant current and a constant power mode. The first one directly feeds the power reference to the current control inputs, corresponding to $[i_{d,\text{ref}}, i_{q,\text{ref}}] = [p_{\text{ref}}, q_{\text{ref}}]$, while the second one adjusts the reference based on voltage measurements such that the DG power output is kept constant, as follows:

$$i_{d,\text{ref}} = \frac{v_d p_{\text{ref}} + v_q q_{\text{ref}}}{v_d^2 + v_q^2}, \quad i_{d,\text{ref}} = \frac{v_q p_{\text{ref}} - v_d q_{\text{ref}}}{v_d^2 + v_q^2}. \tag{27}$$

Note that $i_c^\star = [i_{d,\text{ref}}, i_{q,\text{ref}}]^\mathsf{T}$ in Fig. 3b.

The inner loop outputs the terminal voltage reference, which is combined with the DC-side voltage in order to generate the pulse-width modulation signal. In order to detect the system frequency at the connection terminal, a synchronization unit in the form of a PLL is included in the model of grid-following converters. The complete dynamic model consists of 13 or 15 states, depending on the inverter control type, and is implemented in a rotating dq-frame and in per unit (denoted by lowercase symbols). More details on the overall converter control structure, employed parametrization, potential operation modes and respective transient properties can be found in [14], [16]–[20].

B. LoM Protection Schemes

1) OF/UF Protection Design: The modeling of frequency protection follows the guidelines from [21] and uses additional information provided in [22]–[26]. There are several techniques for determining the frequency signal, namely the zero-crossing methods for obtaining the electrical speed of the synchronous generator [24], approaches based on carrying out continuous Fourier transformation on voltage waveform [25] and PLL-based techniques [26]. A PLL provides fast and robust frequency estimates for balanced three-phase systems and has been widely used for frequency estimation, and is therefore also employed in this study for computing the frequency of the voltage phasor at the connection terminal.

If the frequency signal is not within the prescribed limits $[f_{\min}, f_{\max}]$ and the magnitude of the terminal voltage is larger than the minimum voltage setting $V_{\min}$, the frequency relay sends a trip signal to the generator's circuit breaker. The addition of a voltage amplitude test - a so-called "under-voltage interlock" function - usually ensures the absence of false alarms and restrains the actuation of frequency relays during non-islanding situations such as generator start-up and short circuits [23]. However, since the UV/OV protection schemes are also implemented in this work and the system is

in steady state prior to the LoM event, the voltage amplitude test is redundant and therefore neglected. Moreover, frequency relays can be operated with a time delay in order to avoid false protection tripping during LoM-unrelated transients, since the frequency might exceed the prescribed limits for a short period of time. Under such circumstances, the tripping conditions must persist during a pre-determined period to trigger the relay. Finally, both the protection signal delay, corresponding to circuit breaker opening time, as well as the internal measuring window delay are taken into account [23].

2) OV/UV Protection Design: The generic computational model of the voltage relay employed in this work is similar to the one presented in [25]. First, the voltage of each phase is measured by the PLL and transformed into a synchronously-rotating reference frame, with the phasor amplitude corresponding to the absolute value of the line-to-line Root Mean Square (RMS) voltage. Voltage relays usually calculate the RMS value of the nodal voltage considering a measurement window over a few cycles, and the resulting signal is then low-pass filtered and checked for any violations of the UV/OV settings. However, similarly to the frequency signal, the voltage can also be prone to transient phenomena not produced by an LoM event. Hence, a duration block examining whether the limits are consistently exceeded is incorporated in the model, together with the internal measurement delay and circuit breaker opening time.

3) Protection Settings: For the protection settings, international standards and typical regulations of several countries were followed. The report of British Standard [21] suggests that the frequency response must be activated within $2-5\,\mathrm{s}$, and therefore frequency protection should be able to successfully recognize any LoM event within that time period. It should be noted that in some cases there is a presence of multiple OF/UF protection relays with different delay settings. However, those additional protection layers are primarily designed for extremely narrow limits with significantly higher time duration blocks, corresponding to signals that continuously exceed the predefined thresholds for a duration of up to $30\,\mathrm{min}$. Such example is the United Kingdom, where the $47.5\,\mathrm{Hz}$ under-frequency threshold with $20\,\mathrm{s}$ delay and the $51.5\,\mathrm{Hz}$ over-frequency threshold with $90\,\mathrm{s}$ delay are enforced. As such protection designs require average windows drastically greater than the ones needed for LoM detection, they were not considered in this study. Similar multi-stage OV/UV concepts are also employed for voltage protection, but with settings again mostly outside of the scope of this study. The protection settings used in this work have been selected according to the available standards prescribed by different European system operators in [21] and are listed in Table I.

IV. Results

The proposed analytical approximations are validated through time-domain simulations in MATLAB Simulink, with the single-line diagram of the investigated test system illustrated in Fig. 4. It comprises a $20\,\mathrm{kW}$ DG interfaced via converter to the distribution network, a load supplied locally

TABLE I
EMPLOYED FREQUENCY AND VOLTAGE PROTECTION SETTINGS.

Protection setting type	Frequency	Voltage
Upper threshold (OF/OV)	50.5 Hz	1.1 p.u.
Lower threshold (UF/UV)	49.3 Hz	0.88 p.u.
Internal delay (measuring window)	100 ms	100 ms
Signal delay (breaker opening time)	40 µs	40 µs

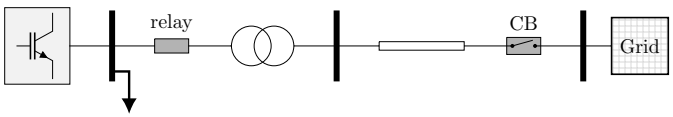

Fig. 4. Single-line diagram of a test system under investigation.

by the DG at the connection terminal, as well as the step-up transformer and distribution feeder connecting the DG to the main grid. The DG operates at $50\,\%$ of its rated power and at the nominal voltage of $400\,\mathrm{V}$. All network components are represented by three-phase models, with feeder and transformer implemented as series impedances. Moreover, the load is modeled as constant RLC load, as this type of load leads to the most conservative islanding detection performance of frequency and voltage-based relays.

The simulated NDZs are obtained in a discretized fashion, as the simulations require re-initialization of the system for different load parameters and result in a binary (i.e., triggered or not) signal output for each protection type. Discrete boundaries of simulated NDZs will be depicted using dots and extrapolated into continuous regions, whereas analytical approximations of the respective thresholds will be represented by full lines. The standard procedure requires $5\,\%$ step-changes in load power in order to evaluate the protection. However, for the purposes of sufficiently accurate comparison, the steps simulated in this study are occasionally significantly smaller and vary from one case to another.

The comparisons between the analytical and simulated NDZs for both the grid-feeding and grid-supporting inverter mode are depicted in Fig. 5. For the grid-feeding case, the power mismatch increments $(\Delta P, \Delta Q)$ were set to $(5, 0.2)\,\%$ for frequency protection validation and $(0.2, 2)\,\%$ for voltage protection analysis, whereas the values used for the grid-supporting mode of operation correspond to $(2.5, 0.5)\,\%$ and $(0.5, 2.5)\,\%$, respectively. The lower discretization is employed in the second case in order to reduce the computational time, as NDZs of grid-supporting DG units are generally larger and greater parameter regions need to be swept. Moreover, the droop gains for the grid-supporting converter type were set to $R_f = 0.7\,\mathrm{p.u.}$ and $R_V = 0.3\,\mathrm{p.u.}$

It is clear that for both operation modes we achieve a

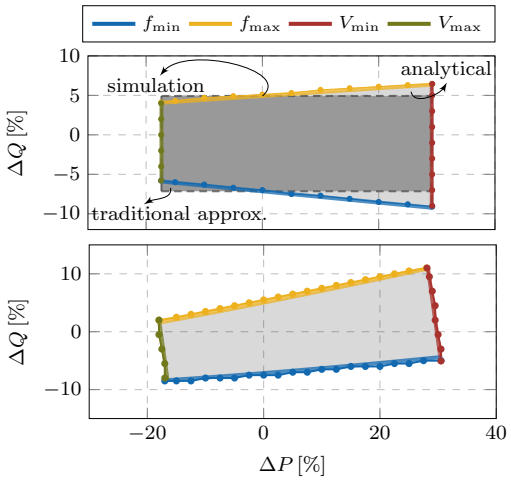

Fig. 5. Comparison of analytical and simulated NDZs in case of grid-following converters: (i) grid-feeding mode; (ii) grid-supporting mode. Dark rectangular region represents an NDZ for the grid-feeding inverter obtained through a traditional approximation.

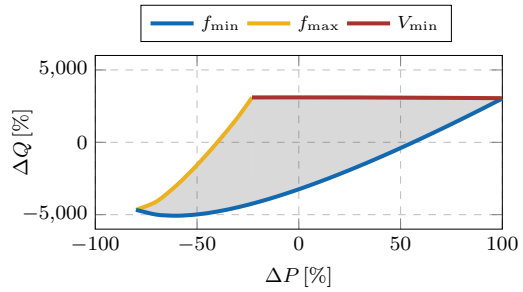

Fig. 6. Analytical NDZ in case of grid-forming converters with conventional droop gain tuning of $(R_P, R_Q) = (0.05, 0.005)$ p.u.

perfect matching between the simulations and the analytical formulation, indicated by the overlap between the full and dotted lines. As previously elaborated in Section II, the lines representing the bounds for frequency protection of grid-feeding converters are also dependent on ΔP and therefore not vertical anymore, resulting in a trapezoidal NDZ. This significantly improves the performance of our approximation compared to the traditional NDZ estimation approach, described by (5) and (9) and indicated by the dark shaded rectangle in Fig. 5. The simulations also validate the accuracy of the novel and more complex NDZ formulation for the grid-supporting converter, with all four NDZ limits being functions of both active and reactive power mismatches. This is particularly important, as grid-supporting requirements are becoming an industry standard and such converter types are rapidly being employed, making the existing NDZ approximations obsolete. Nonetheless, the NDZs of such converter units tend to enlarge dramatically with the increase in droop gains, thus making the LoM protection ineffective. The aforementioned characteristic can be observed in Fig. 7, where the NDZ boundary is presented in the $\Delta P - R_f - \Delta Q$ space for a wide range of frequency droop gains $R_f \in [0-25]$ p.u. It can therefore be concluded that the passive anti-islanding detection schemes based on frequency and voltage triggers might be inadequate for future power systems with high penetration of very responsive grid-supporting DGs, i.e., DG units interfaced through power converters with high droop gains.

On the other hand, the grid-forming mode is characterized by the fact that for conventional droop gains of $(R_P, R_Q) < (0.1, 0.01)$ p.u. the NDZ is rotated by $\approx 90°$ counterclockwise compared to the zones of other inverter modes, as illustrated in Fig. 6. In other words, although typically having $\Delta P - V$ and $\Delta Q - f$ dependencies, the frequency and voltage protection of grid-forming units is mostly affected by the change in ΔP and ΔQ, respectively. However, it should be noted that under traditional droop tuning the non-detection region is extremely

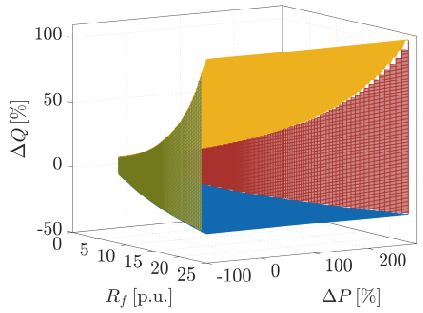

Fig. 7. Analytical NDZ in case of grid-supporting converters for a wide range of frequency droop gains $R_f \in [0-25]$ p.u.

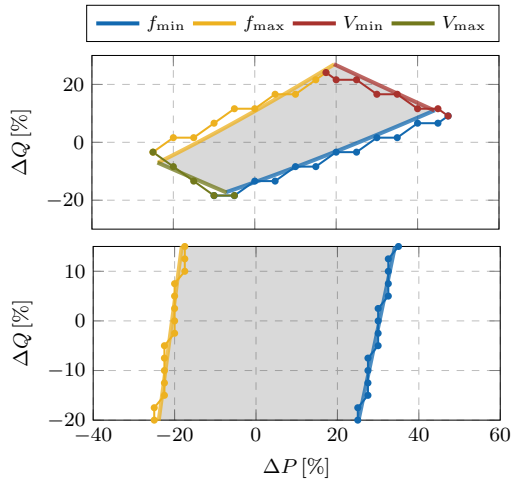

Fig. 8. Comparison of analytical and simulated NDZs in case of grid-forming converters with unconventional droop gain tuning: (i) $(R_P, R_Q) = (0.125, 0.75)$ p.u.; (ii) $(R_P, R_Q) = (0.05, 0.1)$ p.u.

large and almost any type of islanding would go by undetected. This in fact is not a downside, as grid-forming DGs have standalone capabilities by design and should keep energizing the system even after the disconnection from the main grid. Nevertheless, the sole purpose of LoM detection schemes in the presence of grid-forming units is questionable and must be reassessed in the future.

In order to evaluate the proposed analytical approximation for grid-forming DGs, we simulate NDZs for somewhat unconventional droop values of $(0.125, 0.75)$ p.u. and $(0.05, 0.1)$ p.u., since the voltage protection would otherwise never be triggered and the frequency protection would only be activated for a power imbalance of $\Delta P \approx \pm 50\,\%$. The power mismatch steps are set to $5\,\%$ in the first and $2.5\,\%$ in the second case, and the results are presented in Fig. 8. We can confirm that the proposed analytical expressions approximate the corresponding NDZs with sufficient accuracy, as the underlying mismatch is a sole consequence of a less discrete simulation sequence. An interesting observation can be made from the second case study, as the NDZ starts rotating with the droop gains approaching traditionally lower values, implying that only frequency protection preserves sensitivity towards islanding instances.

V. Conclusion

This paper addresses the problem of LoM protection in modern distribution grids, in particular the NDZ approximation of passive anti-islanding detection methods based on OF/UF and OV/UV thresholds. For this purpose, we propose an improved analytical formulation for estimating the NDZ of LoM protection devices in the presence of grid-feeding inverters, which alleviates the imprecision of the existing methods pertaining to the coupling between the frequency and active power mismatch. Furthermore, novel approximations for emerging grid-supporting and grid-forming inverter-based services are also introduced. The analytical results are validated through detailed EMT simulations, suggesting a high accuracy of the proposed formulation. Moreover, some interesting observations regarding the impact of new inverter requirements on the performance of LoM protections have been drawn.

The future work will extend the theoretical analysis onto other passive protection schemes such as anti-islanding detection methods based on RoCoF and voltage phase jumps.

Another interesting avenue for further research is the parallel operation of DGs operating in grid-forming and grid-following modes. In such systems, the voltage and frequency response after the LoM event could be studied using the analytical results proposed in this work.

REFERENCES

[1] "IEEE Standard for Interconnection and Interoperability of Distributed Energy Resources with Associated Electric Power Systems Interfaces," *IEEE Std 1547-2018 (Revision of IEEE Std 1547-2003)*, April 2018.

[2] D. Velasco, C. Trujillo, G. Garcera, and E. Figueres, "Review of anti-islanding techniques in distributed generators," *Renewable and Sustainable Energy Reviews*, vol. 14, no. 6, pp. 1608 – 1614, 2010.

[3] S. K. Manikonda and D. N. Gaonkar, "Comprehensive review of IDMs in DG systems," *IET Smart Grid*, vol. 2, pp. 11–24(13), March 2019.

[4] F. De Mango, M. Liserre, A. Dell'Aquila, and A. Pigazo, "Overview of Anti-Islanding Algorithms for PV Systems. Part I: Passive Methods," in *12th International Power Electronics and Motion Control Conf.*, Aug 2006.

[5] F. De Mango, M. Liserre, and A. Dell'Aquila, "Overview of anti-islanding algorithms for pv systems. part ii: Activemethods," in *12th International Power Electronics and Motion Control Conference*, Aug 2006.

[6] A. Pouryekta *et al.*, "Boundary Detection and Enhancement Strategy for Power System Bus Bar Stabilization - Investigation under Fault Conditions for Islanding Operation," *Energies*, vol. 11, no. 4, pp. 1–22, April 2018.

[7] Shyh-Jier Huang and Fu-Sheng Pai, "A New Approach to Islanding Detection of Dispersed Generators with Self-Commutated Static Power Converters," *IEEE Trans. Power Del.*, vol. 15, no. 2, pp. 500–507, 2000.

[8] Z. Ye, A. Kolwalkar, Y. Zhang, P. Du, and R. Walling, "Evaluation of Anti-Islanding Schemes Based on Nondetection Zone Concept," *IEEE Trans. Power Electron.*, vol. 19, no. 5, pp. 1171–1176, 2004.

[9] R. Teodorescu, M. Liserre, and P. Rodriguez, *Grid Converters for Photovoltaic and Wind Power Systems*. John Wiley & Sons, 2011, vol. 29.

[10] X. Zhu, C. Du, G. Shen, M. Chen, and D. Xu, "Analysis of the Non-detection Zone with Passive Islanding Detection Methods for Current Control DG System," in *2009 Twenty-Fourth Annual IEEE Applied Power Electronics Conference and Exposition*, Feb 2009.

[11] Huili Sun, L. A. C. Lopes, and Zhixiang Luo, "Analysis and comparison of islanding detection methods using a new load parameter space," in *30th Annual Conference of IEEE Industrial Electronics Society, 2004. IECON 2004*, vol. 2, Nov 2004.

[12] M. Bakhshi, R. Noroozian, and G. B. Gharehpetian, "Capability improvement of over/under frequency relays by using a hybrid islanding detection method for synchronous based dg units," in *2012 Proceedings of 17th Conference on Electrical Power Distribution*, May 2012.

[13] M. Yingram and S. Premrudeepreechacharn, "Over/Undervoltage and Undervoltage Shift of Hybrid Islanding Detection Method of Distributed Generation." *Scientific World Journal*, March 2015.

[14] J. Rocabert, A. Luna, F. Blaabjerg, and P. Rodriguez, "Control of Power Converters in AC Microgrids," *IEEE Trans. Power Electron.*, vol. 27, no. 11, pp. 4734–4749, 2012.

[15] "BS EN 62116:2014, Utility-interconnected photovoltaic inverters - Test procedure of islanding prevention measures," British-Standard-Institution, London, Tech. Rep., 2014.

[16] U. Markovic, O. Stanojev, E. Vrettos, P. Aristidou, D. Callaway, and G. Hug, "Understanding Stability of Low-Inertia Systems," *IEEE Transactions on Power Systems*, (under review). [Online]. Available: engrxiv.org/jwzrq

[17] U. Markovic, O. Stanojev, P. Aristidou, and G. Hug, "Partial grid forming concept for 100% inverter-based transmission systems," in *IEEE PES General Meeting*, Aug 2018.

[18] U. Markovic, J. Vorwerk, P. Aristidou, and G. Hug, "Stability analysis of converter control modes in low-inertia power systems," in *2018 IEEE Innovative Smart Grid Technologies - Europe (ISGT-Europe)*, Oct 2018.

[19] I. Caduff, U. Markovic, C. Roberts, G. Hug, and E. Vrettos, "Reduced-Order Modeling of Inverter-Based Generation using Hybrid Singular Perturbation," in *2020 Power Systems Computation Conference (PSCC)*.

[20] R. Ofir, U. Markovic, P. Aristidou, and G.Hug, "Droop vs. virtual inertia: Comparison from the perspective of converter operation mode," in *2018 IEEE International Energy Conference (ENERGYCON)*, June 2018.

[21] "BS EN 50549-1:2019, Requirements for generating plants to be connected in parallel with distribution networks," British-Standard-Institution, London, Tech. Rep., 2019.

[22] J. C. Vieira, W. Freitas, W. Xu, and A. Morelato, "Performance of frequency relays for distributed generation protection," *IEEE transactions on power delivery*, vol. 21, no. 3, pp. 1120–1127, 2006.

[23] A. Hassan and T. A. Kandeel, "Effectiveness of frequency relays on networks with multiple distributed generation," *Journal of Electrical Systems and Information Technology*, vol. 2, no. 1, pp. 75–85, 2015.

[24] C. M. Affonso, W. Freitas, W. Xu, and L. C. P. da Silva, "Performance of rocof relays for embedded generation applications," *IEE Proceedings - Generation, Transmission and Distribution*, vol. 152, no. 1, pp. 109–114, Jan 2005.

[25] J. C. Vieira, W. Freitas, A. Morelato, and J. C. Leao, "Dynamic models of frequency and voltage based relays for distributed generation protection," in *2005 IEEE Russia Power Tech.* IEEE, 2005, pp. 1–5.

[26] V. Kaura and V. Blasko, "Operation of a phase locked loop system under distorted utility conditions," *IEEE Transactions on Industry Applications*, vol. 33, no. 1, pp. 58–63, Jan 1997.

APPENDIX

We explore the monotonic properties of nonlinear functions $g(\cdot)$ and $h(\cdot)$ in Section II-D by analyzing their first derivatives. Let us start with $g(\cdot)$ in (21a) by taking the partial derivative of the right-hand side in (13) with respect to $\hat{V}$ and combining it with (11a), which yields

$$\frac{\partial}{\partial \hat{V}} g\big(V,\hat{V},\Delta Q\big) = -2\frac{V^2 P_{G_1}}{\hat{V}^3 P_G} - \frac{V^2 R_f}{\hat{V}^2 P_G}\frac{\partial}{\partial \hat{V}}\hat{f}\big(V,\hat{V},\Delta Q\big). \tag{28}$$

Here, P_{G_1} denotes the active power of the DG corresponding to frequency deviation Δf_1. The expression for $\xi = \frac{\partial}{\partial \hat{V}}\hat{f}\big(V,\hat{V},\Delta Q\big)$ can be obtained from (19) as follows:

$$\xi = \frac{V R_V}{4\pi C_0 \hat{V}^3}\left(1 + \frac{\beta_V}{2\sqrt{\beta_V^2 + 8\pi f C_0\big(\frac{\Delta Q}{V^2} + 2\pi f C_0\big)}}\right). \tag{29}$$

It can be shown that $\xi \geq 0, \forall \hat{V} \in \mathbb{R}_+$, therefore implying that $\frac{\partial}{\partial \hat{V}} g\big(V,\hat{V},\Delta Q\big) < 0$, i.e., $g\big(V,\hat{V},\Delta Q\big)$ is monotonically decreasing. Hence, for $V_{\min} \leq \hat{V} \leq V_{\max}$ we can state that

$$g_{\min}(V, V_{\max}, \Delta Q) \leq \frac{\Delta P}{P_G} \leq g_{\max}(V, V_{\min}, \Delta Q), \tag{30}$$

which confirms the inequality in (22a).

As for the permissible limits on reactive power mismatch, the partial derivative $\frac{\partial}{\partial \hat{f}} h(f,\hat{f},\Delta P)$ can be derived from (15) and (20) accordingly:

$$\frac{\partial}{\partial \hat{f}} h\big(f,\hat{f},\Delta P\big) = \left(\frac{\Delta P}{P_G} + 1\right)\left(\frac{R R_V f}{\hat{f}^2 \hat{V}\big(f,\hat{f},\Delta P\big)^2}\right. \tag{31}$$
$$\left.\Big(\hat{V}\big(f,\hat{f},\Delta P\big) - V\Big)\left(1 + \frac{\frac{\partial}{\partial \hat{f}}\hat{V}\big(f,\hat{f},\Delta P\big)}{\hat{V}\big(f,\hat{f},\Delta P\big)}\right) + 2Q_f\frac{f^2}{\hat{f}^3}\right).$$

However, unlike the expression in (28), (31) is not monotonic for every system initialization, i.e., it is strictly positive only for $V > \hat{V}$. Nevertheless, after conducting some trivial mathematical transformations, it can be shown that $\frac{\partial}{\partial \hat{f}} h\big(f,\hat{f},\Delta P\big) \geq 0$, $\forall V \in \mathbb{R}_+$ as long as the following inequality holds:

$$2Q_f\frac{f}{\hat{f}} > -\frac{\hat{Q}_G}{\hat{P}_G}\left(1 + \frac{\frac{\partial}{\partial \hat{f}}\hat{V}\big(f,\hat{f},\Delta P\big)}{\hat{V}\big(f,\hat{f},\Delta P\big)}\right). \tag{32}$$

Since typically in practice $\hat{P}_G > \hat{Q}_G$, $0.8 < f/\hat{f} < 1.2$ and $Q_f = 2.5$, the condition in (32) will be satisfied for any realistic DG unit and distribution network under investigation. Therefore, the function $h(f,\hat{f},\Delta P)$ is monotonically increasing on the interval $\hat{f} \in [f_{\min}, f_{\max}]$, which implies that

$$h_{\min}(f, f_{\min}, \Delta P) \leq \frac{\Delta Q}{Q_G} \leq h_{\max}(f, f_{\max}, \Delta P), \tag{33}$$

and hence validates the inequality in (22b).